SEGMENTATION OF THE FETAL ENVELOPE ON ANTE-NATAL MRI

Jérémie Anquez, Lazar Bibin, Elsa D. Angelini, Isabelle Bloch

Institut TELECOM - TELECOM ParisTech - CNRS UMR 5141 LTCI, Paris, France.

ABSTRACT

Recent improvements in MRI scanners have enabled the acquisition of spatially consistent 3D images of the fetus. While recent works focused on the fetal brain segmentation, important outcome could be obtained from the segmentation of the whole fetal body envelope, such as accurate fetal weight estimation. In this paper, we propose to segment this envelope using a semi-automatic approach. MRI images were acquired using the Steady State Free Precession sequence. Taking advantage of the T2-weighting of this sequence, a set of fetal structures is identified and a simplified model of the fetal skeleton is instantiated in the images. An articulated model of a generic fetus is then registered in the images to initialize the fetal envelope segmentation and optimized using graph-cuts to refine the segmentation. Promising and robust results were obtained on a set of nine volumes.

Index Terms— Ante-natal imaging , MRI, fetus segmentation

1. INTRODUCTION

Thanks to higher image quality, shorter acquisition times and whole uterus visibility, MRI constitutes nowadays a good adjunct to echography for pregnancy follow up [1]. As pointed out in [2], a precise estimation of the fetus weight could be derived from the fetal envelope segmentation which is crucial when obstetricians need to plan for an optimal delivery procedure in case of fetal macrosomia (oversized fetuses). However, the few works dedicated to automatize the segmentation of in utero-fetal structures only deal with brain segmentation (see [3, 4]).

In this paper, we propose a semi-automated approach to segment the fetal envelope. To our knowledge, it is the first time this problem is addressed. We consider motion free MRI volumes acquired with the Steady State Free Precession (SSFP) sequence. Fetal motion freezing is possible with this sequence as images including the whole fetus can be obtained in less than 30 seconds [5]. However, the MRI images contain complex information to process, since numerous maternal, uterine and fetal structures are visible, and since the fetus orientation within the uterus (and hence with respect to the acquisition direction) is unknown. The proposed approach to process those images consists in first identifying semi-automatically a set of landmark points located in the fetus to characterize its position in the image (Section 2). Then, an articulated model of the fetus is registered to this skeleton (Section 3), to initialize the fetal envelope segmentation (Section 4).

This work was partially funded by Orange Labs R&D and Fondation Santé et Radiofréquences (FEMONUM project). The authors thank the members of C. Adamsbaum's group, Department of Radiology, St Vincent de Paul Hospital, Paris, France, for providing the MRI data and their medical expertise.

2. CHARACTERIZATION OF THE FETAL POSITION

Data acquisition. 24 MRI volumes of fetuses between 30 and 35 gestational weeks were collected. All the images were acquired with the SSFP sequence on a 1.5 Tesla superconducting units (Avanto, General Electric^{TM}, Milwaukee (WI), United States). Typical acquisition parameters were: TR/TE = 4.2/1.8 ms, flip angle = 60°, FOV = 480, slice thickness/gap = 4/0 mm, matrix = 512×512, while voxel size were 0.94 x 0.94 x 4 mm^3.

Simplified model of the fetus skeleton. To characterize the fetus position, we instantiate a model of its skeleton S, shown in Figure 1. As the real skeleton includes more than 270 bones, which are not all involved in the fetus positioning, we propose a simplified skeleton S, composed of a reduced set of 20 pseudo-bones O_i.

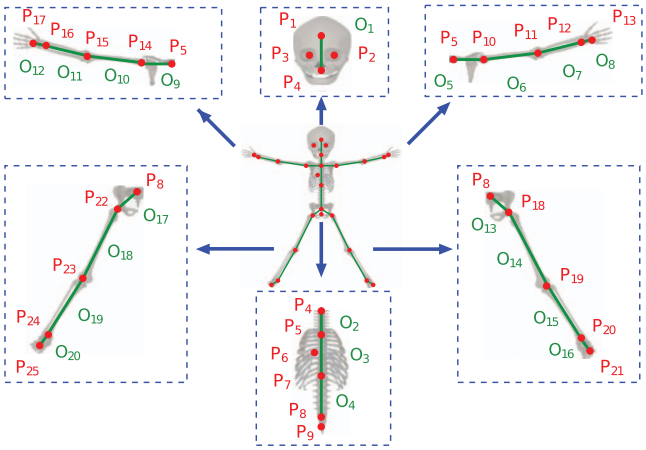

Fig. 1. Simplified model of the fetus skeleton S.

Landmark points detection. To instantiate S in an image, we need to determine the position, the scale and the orientation of the O_i. This is performed by detecting a set of landmark points P_j, which define the position of different bone structures. This set is composed of the O_i extremities, together with anatomical points used to define the O_i orientation. Since bones are not well contrasted on images acquired with the SSFP sequence, some bone structures cannot be depicted precisely in the images. Anatomical structures contained in the bone structures are segmented as a surrogate, to define indirectly their location. For instance, the urinary bladder determines implicitly the location of the pelvis. The complete list of the P_j is given in Table 1, with the bone structures they identify and the anatomical structures that are to be detected.

To guide the segmentation of the different anatomical structures, we take advantage of the T2 weighting of the SSFP sequence. In the images acquired with this sequence, physiological liquids (high intensity) greatly contrast with the neighboring bones or soft tissues

Id	Bone structure	Anatomical structure
P_1	skull	skull bone content
P_2, P_3	orbits	eyes
P_4	1st cervical vertebra	skull bone content
P_5	7th cervical vertebra	spinal canal
P_6	rib cage	lungs
P_7	10th thoracic vertebra	spinal canal
P_8	sacrum	spinal canal
P_9	pelvis	urinary bladder
P_{10}, P_{14}	humeral heads	humeral heads
P_{11}, P_{15}	elbows	elbows
P_{12}, P_{16}	wrists	wrists
P_{13}, P_{17}	metacarpi	metacarpi
P_{18}, P_{22}	femoral heads	femoral heads
P_{19}, P_{23}	knees	knees
P_{20}, P_{24}	ankles	ankles
P_{21}, P_{25}	metatarsi	metatarsi

Table 1. Correspondence between the bone structures containing the P_j and the anatomical structures detected in the images.

(low intensity), as shown in Figure 2. For instance, the skull bone content, which is composed of the brain and the cerebrospinal fluid, highly contrasts with the skull surrounding it.

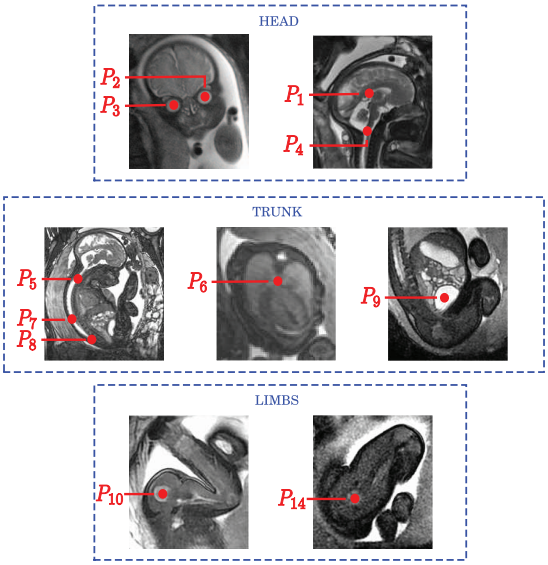

Fig. 2. Fetal anatomical structures detected and corresponding P_j.

The anatomical structures segmentation is performed through an exploration of the fetus anatomy, starting from the head, propagating to the trunk and ending with the limbs. The eyes and the skull bone content are segmented automatically, exploiting the method described in [6]. It consists in identifying the fetus eyes using a template matching approach. The eyes location is then used to segment the skull bone content in a reconstructed sagittal slice and, eventually, in the 3D image. Landmark points are extracted from the segmentation results: P_2 and P_3 correspond to the eyes centers, P_1 to the center of gravity of the skull bone content and P_4 to the spinal canal root.

The exploration process deals next with the structures located in the fetal trunk. The centerline of the spinal canal is identified by extracting the shortest path between P_4 and P_8 (manually selected in the fetus sacrum) with the approach described in [7]. A graph of the image is built, with nodes corresponding to the image voxels. Edges between neighboring voxels are added. The weighting w_{pq} of the edge e_{pq} linking two voxels v_p and v_q is equal to $1/I_q$, where $I(q)$ is the intensity of v_q. This aims at favoring the inclusion of voxels located in the spinal canal, which is filled with highly intense cerebrospinal fluid. This process was successful on all the images, the extracted path being entirely contained in the spinal canal in all cases. The points P_5 (7th cervical vertebra) and P_7 (10th thoracic vertebra) are identified based on their distance to P_4 along the centerline, following biometric information from [8]. A thoracic plane, orthogonal to the centerline in its superior part, is reconstructed and P_6 is selected manually at the junction of the lungs. Finally, P_9 is selected manually within the urinary bladder.

Landmark points located in the fetus articulations (P_{10} to P_{25}) are all selected manually. Articulations are made of cartilage, which have a higher intensity than the neighboring soft tissues, thus making possible their identification (see Figure 2). The selection process was repeated twice by the same operator in all images. Reasonable repeatability was observed, as the mean distance between the points obtained in the two tests was inferior to 5 mm in 3D.

Instantiation of S in the images. The set of P_j is exploited to determine the position, the scale and the orientation of the $O_i = (P_k, P_l)$. The position is given by the location of its first extremity P_k, while the scale corresponds to the distance $||\overrightarrow{P_k P_l}||$. The orientation is defined by an orthonormal basis $\mathcal{B}_i = (\overrightarrow{o_{i,1}}, \overrightarrow{o_{i,2}}, \overrightarrow{o_{i,3}})$. The first element $\overrightarrow{o_{i,1}} = \frac{\overrightarrow{P_k P_l}}{||\overrightarrow{P_k P_l}||}$ corresponds to the axial direction of O_i. The roll around the pseudo-bone axis is defined by $\overrightarrow{o_{i,2}} = \frac{\overrightarrow{P_m P'_m}}{||\overrightarrow{P_m P'_m}||}$, where P_m is a complementary landmark point and P'_m is its projection on $\overrightarrow{o_{i,1}}$. For instance, the roll of $O_3 = (P_5, P_7)$, corresponding to the thoracic part of the spine, is defined using $P_m = P_6$. This is adequate as P_6 is located at the lung junction, which defines implicitly the position of the rib cage. The basis is completed by $\overrightarrow{o_{i,3}} = \overrightarrow{o_{i,1}} \wedge \overrightarrow{o_{i,2}}$. The list of the pseudo-bones $O_i = (P_k, P_l)$ and the corresponding P_m is given in Table 2.

O_i	(P_k, P_l)	P_m
O_1	(P_1, P_4)	P_2
O_2	(P_4, P_5)	P_6
O_3	(P_5, P_7)	P_6
O_4	(P_7, P_8)	P_9
O_5, O_9	$(P_5, P_{10}), (P_5, P_{14})$	P_6,P_6
O_6, O_{10}	$(P_{10}, P_{11}), (P_{14}, P_{15})$	P_{12},P_{16}
O_7, O_{11}	$(P_{11}, P_{12}), (P_{15}, P_{16})$	P_{13},P_{17}
O_8, O_{12}	$(P_{12}, P_{13}), (P_{16}, P_{17})$	P_{11},P_{15}
O_{13}, O_{17}	$(P_8, P_{18}), (P_8, P_{22})$	P_9,P_9
O_{14}, O_{18}	$(P_{18}, P_{19}), (P_{22}, P_{23})$	P_{20},P_{24}
O_{15}, O_{19}	$(P_{19}, P_{20}), (P_{23}, P_{24})$	P_{18},P_{22}
O_{16}, O_{20}	$(P_{20}, P_{21}), (P_{24}, P_{25})$	P_{19},P_{23}

Table 2. List of the pseudo-bones O_i and complementary landmark point P_m used to define the vectors $o_{i,2}$ for each $O_i = (P_k, P_l)$.

3. ARTICULATED MODEL REGISTRATION

Articulated model construction. To initialize the fetal envelope segmentation, we rely on an articulated model of a generic fetus.

This model was built from an image containing a fetus representative of our database: (1) the image was acquired at 32 gestational weeks, which approximatively corresponds to the mean age of the fetus in our database, and (2) the fetus position was typical as shown in Figure 3. The fetus was segmented manually into 6 parts (head, trunk, arms and legs), to disconnect easily the limbs from the head and trunk, and the surface of each part was meshed.

The skeleton model, denoted S_m, was instantiated in the image to articulate the fetus model. This operation was performed using the software Blender (http://www.blender.org), which provides utilities to animate virtual characters. The skeleton S_m was imported into Blender, to realize the "skinning" of the fetus model. It consists in defining an association degree between the fetus model vertices and the different O_i of S_m. Consequently, a spatial transform applied to a given O_i will be indirectly applied to its associated vertices [9].

Model registration. To embed the articulated fetus model in an image I, its skeleton S_m is registered to the skeleton S_I extracted from the image. It is achieved by registering each pseudo-bone of S_m to its counterpart in S_I. To do so, a linear transform T_i is determined for each O_i, using its position, scale and orientation in S_m and S_I, to minimize the distance between O_i in S_m and its counterpart in S_I while preserving the articulations (i.e. topology of the skeleton). This process is synthesized in Figure 3.

After registration, deformed models are finally rasterized to create a binary mask. This process was evaluated on four MRI datasets for which a manual segmentation of the fetus, performed by an obstetrician, was available. A mean overlap of 74 % was obtained, showing a satisfying initial correspondence between the registered model and the manual segmentation.

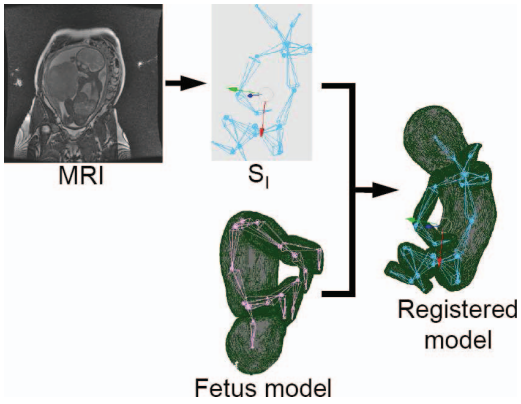

Fig. 3. Articulated fetus model positioning. The articulated model is deformed by registering its skeleton S_m (in pink) to the skeleton S_I (in blue) extracted from an MRI volume.

4. FETAL ENVELOPE SEGMENTATION

Although the registration provides a quite satisfactory segmentation, this result can be further refined by using the whole image information. We propose a graph-cut approach to achieve this aim.

Search region. Using the result of the articulated model registration, we define a narrow band NB to constrain the segmentation of the fetal envelope, as illustrated in Figure 4. This narrow band must include the whole fetal envelope and is defined as $NB = R_e \backslash R_i$, where R_i and R_e must be included and contain the fetal envelope, respectively. R_i results from the union of the segmented anatomical structures (skull bone content and eyes), the fetus skeleton (where bones are represented by cylinders of diameter 5 mm) and the result of the erosion of the registered articulated model. R_e corresponds to the result of the dilation of the registered articulated model, from which voxels superior to P_1 and separated by more than 8 mm from the skull bone content have been excluded. This prevents from including maternal structures into the search region. Indeed, the inclusion of the urinary bladder into NB when the fetus is in cephalic position can generate some leakage in the segmentation results.

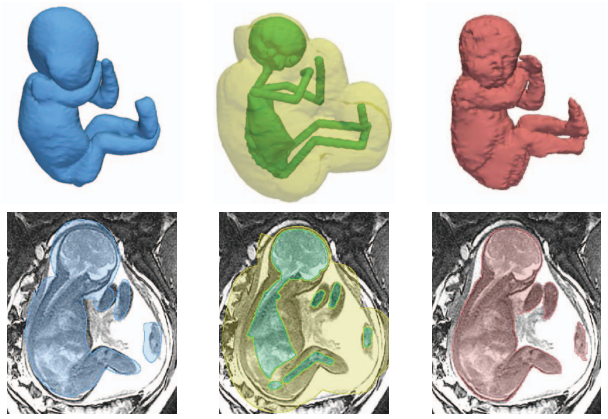

Fig. 4. Segmentation of the fetal envelope. (a) Registered articulated model, (b) constructed narrow band (with R_i in green and R_e in yellow), (c) segmentation result.

Fetal envelope segmentation. A graph cut segmentation is performed inside NB [10]. Oriented edges are created between neighboring pixels. Two special nodes, the source S and the sink T, are added. Edges are created between (1) S and the pixels of NB adjacent to R_i and (2) T and the pixels of NB adjacent to R_e. The minimal cut of the graph provides a binary segmentation corresponding to a minimal surface in the region located between the source and the sink, based on the edge weights. Let p and q be two neighboring voxels and I_p and I_q their intensity. The weight of the edge linking p to q is defined as $w_{pq} = e^{-(I_p - I_q)^2/2\sigma^2}/dist(p,q)$, if $I_p < I_q$, and $w_{pq} = 1/dist(p,q)$ otherwise. This weighting includes contrast prior information, as proposed in [11]. Since soft tissues are darker than the amniotic fluid due to the T2 weighting of the SSFP sequence, edges linking soft tissues voxels to amniotic fluid pixels have a low weight, making them prone to belong to the minimal cut (see Figure 3 (c)).

Segmentation results were quantitatively evaluated on four datasets, using $\sigma = 10$ in all experiments. The mean distance md and the kappa measure κ were computed between the segmentation results and the manual segmentations. The mean values for each indicator are noted μ_{md} and μ_κ respectively. We obtained $\mu_{md} = 1.4$ mm and $\mu_\kappa = 0.89$, confirming a good overall agreement between manual and automatic segmentations of the fetal envelope. The best ($md = 0.9$ mm and $\kappa = 0.93$) and worst results ($md = 2.0$ mm and $\kappa = 0.84$) are shown in Figure 5. Both results are acceptable but only local defects are visible on the former, while several maternal structures are aggregated to the latter.

The whole segmentation process takes about 12 minutes (10 for landmark points selection, 2 for registration and envelope segmen-

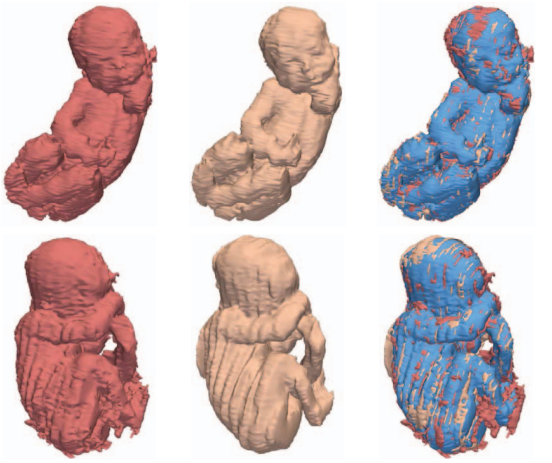

(a) (b) (c)

Fig. 5. Comparison of the segmentation result with ground truth, for the best (top) and worst results (bottom). (a) Automatic segmentations, (b) manual segmentations, (c) differences (blue: correct segmentation, red: false positives, pink: false negatives).

tation) on a 3.5 GHz PC running MATLAB (The MathWorks Inc.). An important time gain is observed, compared to the hour needed to segment the fetal envelope in [2] with comparable data. This amount of time seems compatible with clinical use, when precise fetus segmentation is needed for appropriate planning of delivery.

5. CONCLUSION

A semi-automatic method is proposed to segment the fetal envelope on ante-natal MRI. A simplified skeleton is first extracted from the images, identifying a set of 25 landmark points. Then, an articulated model of a generic fetus is registered to this skeleton. Finally, the registration result is used to define a narrow-band containing the fetal envelope, which is segmented using a graph-cut approach. Precise results were obtained on four datasets using this method, which can be used for fetal weight estimation.

The segmentation results were refined by identifying several fetal organs in the MRI volumes (brain, lungs, heart, stomach, urinary bladder), to elaborate anatomically detailed utero-fetal unit models. Each model was embedded into a synthetic woman body to build a set of pregnant woman models at different stages of pregnancy [12]. Dosimetry studies have been performed using these models, to study the influence of electromagnetic fields on the fetus.

Fig. 6. Results obtained on images acquired with the SSFP 3D sequence.

This approach has been also tested on images acquired with the 3D version of the SSFP sequence. Since those images have high spatial resolutions (voxel size is 1.6 x 1.6 x 1.4 mm^3), several hours would be needed to manually segment the fetal envelope while processing time remains stable using our approach. Promising results were obtained on this data, as shown in Figure 6. While not validated quantitatively, the 3D reconstructions allowed to clearly depict the fetus morphology. These results open the way for new clinical applications, such as facial features analysis.

The processing time could be reduced by increasing the automation of the landmark point selection process, especially regarding the articulations identification. Prior knowledge such as contrast, shape modeling and/or biometric information could be exploited to guide the segmentation and to obtain more reproducible results. An extended validation on the whole available database remains necessary to evaluate the robustness of the method.

6. REFERENCES

[1] D. Prayer and P.C. Brugger, "Investigation of normal organ development with fetal MRI," *European Radiology*, vol. 17, no. 10, pp. 2458–2471, 2007.

[2] S. Hassibi, N. Farhataziz, M. Zaretsky, D. McIntire, and D.M. Twickler, "Optimization of Fetal Weight Estimates Using MRI: Comparison of Acquisitions," *American Journal of Roentgenology*, vol. 183, no. 2, pp. 487–492, 2004.

[3] A. Cachia, J.F. Mangin, D. Riviere, F. Kherif, N. Boddaert, A. Andrade, D. Papadopoulos-Orfanos, J.B. Poline, I. Bloch, M. Zilbovicius, et al., "A primal sketch of the cortex mean curvature: a morphogenesis based approach to study the variability of the folding patterns," *IEEE Transactions on Medical Imaging*, vol. 22, no. 6, pp. 754–765, 2003.

[4] P.A. Habas, K. Kim, F. Rousseau, O.A. Glenn, A.J. Barkovich, and C. Studholme, "Atlas-based segmentation of the germinal matrix from in utero clinical MRI of the fetal brain," in *MICCAI*, 2008, vol. LNCS 5241, pp. 351–358.

[5] J. Anquez, E. Angelini, I. Bloch, V. Merzoug, A. E. Bellaiche-Millischer, and C. Adamsbaum, "Interest of the Steady State Free Precession (SSFP) sequence for 3D modeling of the whole fetus," in *EMBC*, 2007, pp. 771–774.

[6] J. Anquez, E. Angelini, and I. Bloch, "Automatic segmentation of head structures on fetal MRI," in *ISBI*, Boston, USA, June 2009, pp. 109–112.

[7] E.W. Dijkstra, "A Note on Two Problems in Connexion with Graphs," *Numerische Mathematik*, vol. 50, pp. 269–271, 1959.

[8] H. Gray and S. Standring, *Gray's anatomy: the anatomical basis of clinical practice*, Churchill Livingstone, 2005.

[9] I. Baran and J. Popović, "Automatic rigging and animation of 3d characters," in *Proceedings of the 2007 SIGGRAPH conference*, 2007.

[10] Y. Boykov, O. Veksler, and R. Zabih, "Fast Approximate Energy Minimization via Graph Cuts," *IEEE Transactions on Pattern Analysis and Machine Intelligence*, pp. 1222–1239, 2001.

[11] Y. Boykov and G. Funka-Lea, "Graph Cuts and Efficient NDImage Segmentation," *International Journal of Computer Vision*, vol. 70, no. 2, pp. 109–131, 2006.

[12] J. Anquez, T. Boubekeur, L. Bibin, E. D. Angelini, and I. Bloch, "Utero-fetal unit and pregnant woman modeling using a computer graphics approach for dosimetry studies," in *MICCAI*, 2009, vol. LNCS 5761, pp. 1025–1032.